Available online at www.sciencedirect.com
SCIENCE DIRECT
Polymer 47 (2006) 5161–5173
polymer
www.elsevier.com/locate/polymer

Synthesis and crystallization kinetics of silsesquioxane-based hybrid star poly(ε-caprolactone)

Jianwen Xu, Wenfang Shi *

State Key Laboratory of Fire Science, Department of Polymer Science and Engineering, University of Science and Technology of China, Hefei, Anhui 230026, People's Republic of China

Received 22 February 2006; received in revised form 6 April 2006; accepted 28 April 2006
Available online 26 May 2006

Abstract

A series of silsesquioxane-based hybrid star poly(ε-caprolactone) with different arm length (SHPCL-4, SHPCL-10, SHPCL-40) were synthesized from ring-opening polymerisation of ε-caprolactone as a monomer initiated by silsesquioxane-based hybrid polyol (SBOH). Two linear poly(ε-caprolactone)s, LPCL-25 and LPCL-35, were also prepared for comparison. The sequence of LPCL-25 < LPCL-35 < SHPCL-4 < SHPCL-10 < SHPCL-40 for total molecular weights (M_n) and the sequence of SHPCL-4 < SHPCL-10 < LPCL-25 < LPCL-35 < SHPCL-40 for average molecular weight per arm (M_{arm}^{NMR}) were determined by ^{1}H NMR and GPC measurements. The ^{1}H NMR data also suggested that SHPCLs possess a spheric architecture with 29.2 arms in average. The crystallization kinetics study by non-isothermal DSC showed that the starting temperature of crystallization (T_s), the ending temperature (T_e) and the peak temperature of exothermic curve (T_p) are in the order as: SHPCL-4 < SHPCL-10 < LPCL-25 < SHPCL-40 ≈ LPCL-35, while the crystallinity (X_c) follows the order of SHPCL-4 < SHPCL-10 < SHPCL-40 < LPCL-25 < LPCL-35. The corrected overall crystallization rate constant (K_c) calculated from Avrami equation were found to be in the order as: SHPCL-4 < SHPCL-10 < LPCL-35 < LPCL-25 ≈ SHPCL-40, which was further evidenced by the real time morphological observation with polarized light microscopy (POM). It is also found by the POM measurements that the inorganic core and star architecture greatly retards the nucleation of SHPCLs with short arms, while it helps the nucleation of SHPCL with longer arms.

Keywords: Star polymer; Crystallization; DSC

1. Introduction

Poly(ε-caprolactone) (PCL) is a crystalline polymer with a glass transition temperature of about −60 °C. Linear PCL (LPCL) usually has a melting temperature of 59–64 °C, depending on its molecular weight. PCL is one of the most extensively studied and most widely used aliphatic polyesters, mainly due to its miscibility with different commercial polymers (SAN, ABS, PVC, nitrocellulose), ability to disperse pigments, low-temperature adhesiveness, and biocompatibility and biodegradability [1]. PCL is attracting interest especially in drug delivery systems and scaffolds for tissue engineering [2–5]. However, the mechanical brittleness at physiologic temperature and in vitro or in vivo inhomogeneous degradation behaviours due to the high crystallinity limit its further applications. A great number of research have been done to reduce the crystallinity of PCL, such as through copolymerization of ε-caprolactone and other cyclic monomers [6–9], block extension with ester or urethane bonds [10,11], and introduction of branched structures [12–14], etc.

Highly branched polymers, such as star-shaped polymers, dendrimers, and hyperbranched polymers, have shown unique properties compared with their linear counterparts due to their higher segment density within the distance of gyration radius [15,16]. They usually possess smaller hydrodynamic radius, and lower melting and solution viscosity. The branched architecture also has great influence on the packaging of molecular chains [17]. Ascribing to their unique structures, some star-shaped, dendritic and hyperbranched PCLs have been synthesized and used as precursors for powder coatings [13,14], hydrogels [18] and templates for preparing nanoparticles [19]. The crystallization kinetics of PCL in semi-crystalline polymer blends has been extensively studied in recent years [20], and found that the crystallization process has great influence on the final mechanical properties of blends [21–23]. There are a few papers concerning the crystallization of PCL with star-shaped, dendritic or hyperbranched

* Corresponding author. Tel.: +86 551 3606084; fax: +86 551 3606630.
E-mail address: wfshi@ustc.edu.cn (W. Shi).

0032-3861/$ - see front matter © 2006 Elsevier Ltd. All rights reserved.
doi:10.1016/j.polymer.2006.04.062

architectures [13,24,25]. However, all of them dealt with pure organic systems up to now.

Organic/inorganic hybrid materials have achieved great success in the last decades due to the synergetic effect of organic and inorganic components in nanoscales [26–28]. Organic/inorganic PCL hybrid materials have been prepared through sol–gel method or by intercalation of layered silicate by several groups [29–32]. Their mechanical properties and the crystallinity of PCL in inorganic silica network were studied. However, PCL/silica hybrids with well defined architecture and multi-functional groups for further modification are more desired. Recently, Chang et al. prepared organic/inorganic hybrid star PCL based on nanostructured polyhedral oligomeric silsesquioxanes, and studied their inclusion complexes with cyclodextrin [33].

For obtaining organic/inorganic hybrid materials with best synergetic effect, further study about the influence of inorganic components on organic polymeric chains at nanoscale dimensions is needed. In this work, a series of well defined organic/inorganic hybrid star PCL were prepared through ring-opening polymerisation (ROP) of CL initiated by silsesquioxane-based nanoparticles with a high density of hydroxyl groups on the surface (58 hydroxyl groups per nanoparticle).The synthesized multifunctional star hybrid PCL containing inorganic silsesquioxane core possess potential as starting materials for the applications in tissue engineering and drug delivery systems. It is expected that the inorganic core and star architecture may disrupt the orientation of PCL chains and lead to PCL having high molecular weight PCL with low crystallinity. The crystallization kinetics of such prepared organic/inorganic hybrid star PCL was studied to illustrate the influence of inorganic core and star architecture on PCL arms.

2. Experimental section

2.1. Materials

3-Aminopropyltriethoxysilane and glycidol were purchased from Sigma–Aldrich and used as received. ε-Caprolactone supplied by Sigma–Aldrich was distilled over calcium hydride under reduced pressure, and then kept with 4 Å molecular sieve in a desiccator. The stannous octoate ($Sn(Oct)_2$) and ethylene glycol were supplied by Shanghai First Reagent Co. (China), and distilled under reduced pressure before use. Tetrahydrofuran (THF) and methanol were used as received with analytical grade.

2.2. Synthesis

2.2.1. Silsesquioxane-based polyol (SBOH)

The starting silsesquioxane-based polyol (SBOH) was prepared according to the procedure developed by Mori et al. [34,35]. 287.82 g (1.558 mol) the adduct of 3-aminopropyltriethoxysilane and glycidol according to the ratio of 1:2 was dissolved in 1400 ml methanol, then 42.06 g aqueous HF solution (3.225%) was introduced. After stirring for 4 h at ambient temperature, the reactant was distilled under vacuum to remove water, ethanol and methanol, and then dried at 40 °C in vacuum for 72 h, resulting in a glassy solid at room temperature, named SBOH.

2.2.2. Silsesquioxane-based star hybrid poly(ε-caprolactone) (SHPCL)

The obtained SBOH was used as an initiator for ROP of CL monomer (Scheme 1). The different molar ratios of CL to SBOH (Table 1) were employed to prepare star polymers with different molecular arm length and thus different molecular weights. The following is a representative procedure: 5.260 g SBOH (81.515 mmol –OH) was melted in a flame-dried 50 ml round-bottom bottle at 130 °C in nitrogen atmosphere, and then degassed under reduced pressure for 4 h. 35.952 g CL (314.982 mmol) was introduced into the melted SBOH at 150 °C to form a homogenous and transparent solution. After the solution was cooled down to room temperature, a catalytic amount of $Sn(Oct)_2$ (0.255 g, 0.630 mmol) was injected. The reactant solution was stirred at 140 °C for 20 h under nitrogen atmosphere. The resultant product was dissolved in a large amount of THF and precipitated from cold methanol in order to remove un-reacted CL and the catalyst. This procedure was repeated for three times. The final yields were about 80–95% for different CL/OH ratios. The obtained pale yellow or white powders were kept at 40 °C in vacuum oven for 4 days before measurements.

Table 1
Molecular weights and melting points of SHPCLs and LPCLs

Sample	[CL]/[OH][a]	M_n^{theo}[b]	M_{arm}^{NMR}[c]	M_n^{NMR}[c]	M_n^{GPC}[d]	PI.[d]	T_m (°C)[e]
SHPCL-4	4.0	30,368	1301	41,749	26,016	1.60	47.0
SHPCL-10	10.0	70,290	3139	95,419	44,464	2.28	52.8
SHPCL-40	40.0	269,840	10,318	305,046	106,765	3.13	57.7
LPCL-25	25.0	5769	6694	6694	10,746	1.22	52.7
LPCL-35	35.0	8052	9650	9650	17,341	1.35	55.5

[a] The molar ratio of ε-caprolactone to hydroxyl group.
[b] Theoretical total molecular weight per molecule (M_n^{theo}).
[c] Average molecular weight of each arm (M_{arm}^{NMR}) and total molecular weight per molecule (M_n^{NMR}), calculated from NMR measurements.
[d] Number-average molecular weight (M_n^{GPC}) and polydispersity index (PI.) measured by GPC.
[e] Measured from the peak temperature of endothermal curves in DSC heating at 10 °C/min.

2.2.3. Linear poly(ε-caprolactone) (LPCL)

The procedure for preparing LPCL was almost the same as that for SHPCL. Freshly distilled ethylene glycol and CL with different ratios (Table 1) were introduced into a 50 ml round bottom, a catalytic amount of $Sn(Oct)_2 \cdot (Sn(Oct)_2/CL = 1/500)$ was added and then sealed in nitrogen atmosphere. The reactant was stirred at 140 °C for 20 h before purification. The resulted white powders were kept at 40 °C in vacuum oven for 4 days before measurements.

2.3. Measurements

The NMR experiments were carried out on a Bruker 300 MHz nuclear magnetic resonance instrument using D_2O or $CDCl_3$ as solvents and tetramethylsilane as an internal reference.

The number-average molecular weight M_n and molecular weight distribution (M_w/M_n) were determined using a Waters 150 C gel permeation chromatograph (GPC) equipped with UltraStyragel columns (pore sizes 10^3, 10^4 and 10^5 Å) and a 410 refractive index detector. The narrow-polydispersity polystyrene standards were used in the calibration, and THF was the eluent at a flow rate of 1.0 mL/min.

The differential scanning calorimetry (DSC) measurements were made on a Perkin–Elmer Diamond differential scanning calorimeter under a dry nitrogen atmosphere. Indium and tin standards were used for calibration in low and high temperature regions, respectively. Indium ($\Delta H = 28.45$ J/g) was also used for heat flow calibration. For the measurement of melting point (T_m), the sample was heated from −20 to 100 °C with a heating rate of 10 °C/min and the peak temperature of endothermal curve was taken as T_m. For the non-isothermal crystallization measurements, a typical experimental procedure was as follows: about 5 mg sample was weighed into a DSC pan, and then heated to 100 °C at a heating rate of 10 °C/min and kept for 3 min to destroy any thermal history; subsequently it was cooled down to 0 °C at a constant cooling rate and the crystallization exothermal curves were recorded. Each sample was measured at five different cooling rates (10, 8, 6, 4, and 2 °C/min, respectively), to study its crystallization kinetics. Each thermal treatment was repeated for three times to assure the reproducibility.

The spherulite growth process and the developed crystal morphology were observed on an Olympus polarized optical microscopy (POM) with BX51 M system, which is equipped with a Mettler Toledo FP82HT hot stage and a Mettler Toledo FP90 controller. The samples were firstly melted between two glass slides at 100 °C for 10 min in a hot stage and then transferred fleetly into another hot stage in the microscopy, which was preheated and kept at 40 °C. The digital images of crystallization process were recorded with the integrating BX51 M video camera system and further analyzed by Photoshop software to calculate the size of spherulites.

3. Results and discussion

3.1. Synthesis and architecture characterization

Multi-functional polyol SBOH was prepared by hydrolysis and condensation of an organic silane, *N*,*N*-di(2,3-dihydroxypropyl)-(aminopropyl)triethoxysilane ($(CH_3CH_2O)_3SiCH_2CH_2CH_2N(CH_2CH(OH)CH_2OH)_2$) according to the method developed by Mori et al. [34,35]. SBOH is a sphere-shaped nanoparticle with a diameter of about 2.7 nm, and consists of the species having 12–18 Si atoms with cage-like structures of Si–O–Si and Si–O–C bonds [34,35]. Moreover, the molecular weight and polydispersity index of SBOH were 3760 g/mol and 1.21, respectively. Since the molecular weight and hydroxyl groups number per unit containing one Si atom are 258.3 and 4, respectively, so the average unit number per SBOH is 14.6 (3760/258.3), and thus totally about 58 hydroxyl groups on the surface per SBOH were obtained by calculation. Due to the inorganic characteristic of Si–O–Si in the core and a lot of active –OH groups on the surface, SBOH can be used as a good platform for studying the interaction between inorganic core and branched arms after appropriate modification. In this work, SBOH was employed as an initiator for ring-opening polymerisation of CL.

Due to the high density of hydrophilic hydroxyl groups on the surface, SBOH is a highly hygroscopic material and is soluble just in strong polar solvents, such as water, methanol, *N*,*N*-dimethyl acetamide and dimethylsulfone, it was unsuccessful to obtain PCL with reasonable molecular weight distribution by ROP of CL in solution initiated by SBOH. Bulk polymerisation of CL was chose in this work. $Sn(Oct)_2$ is an effective catalyst in ROP of various lactones and lactides capable of producing high yield and high molecular weight. The molar ratio of $CL/Sn(Oct)_2$ was fixed as 500 in all recipes. To obtain SHPCL with different molecular weights, the molar ratio of CL/OH was varied. The composition and molecular weight were characterized by ^1H NMR spectroscopy (Fig. 1 and Table 1) and GPC (Fig. 2). For SHPCL, the average arm number attached to each SBOH (N_{arm}) and the average length per arm (N_{CL}) are two important parameters. The ratio of integration area of the peak corresponding to methylene groups at the arm ends (–CH_2OH, δ 3.50–3.66, f in Fig. 1(b)) to that of the peak corresponding to the methylene groups near Si atoms in silsesquioxane core (–Si–CH_2–, δ 0.40–0.85, k in Fig. 1(b)) was 2.0 in all the synthesized SHPCL samples, indicating that two PCL arms were initiated from one Si unit, so the N_{arm} was 29.2 since there were average 14.6 Si units per SBOH. The 50% initiating degree of hydroxyl groups in SBOH molecule can be ascribed to the difference of reactivity between primary and secondary hydroxyl groups and the steric hindrance of growing PCL chains. Since the ratio of integration area of the peak corresponding to methylene groups in CL units (–$COCH_2$–, δ 2.40–2.70, $b + b'$ in Fig. 1(b)) to that of the peak corresponding to the methylene groups in silsesquioxane core c(–Si–CH_2–, δ

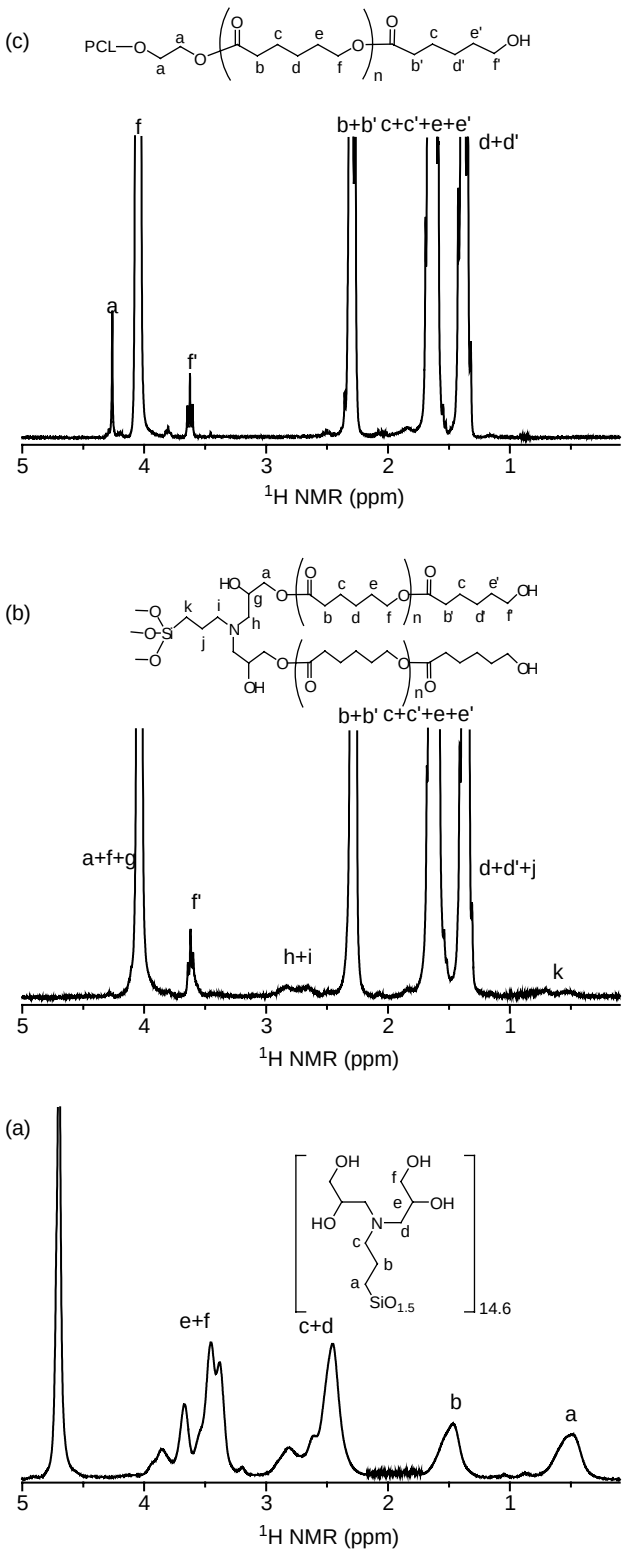

Fig. 1. ^{1}H NMR of (a) SBOH in D_2O, (b) SHPCL-4 in $CDCl_3$, and (c) LPCL-35 in $CDCl_3$.

0.40–0.85, k in Fig. 1(b)) is the degree of polymerisation of CL per Si unit, from which two arms are growing, N_{CL} can be calculated according to $N_{CL}=I_{b+b'}/2I_k$. Accordingly, the average molecular weight of each arm (M_{arm}^{NMR}) can be calculated by $N_{CL}\times 114.14$, in which 114.14 is the molecular weight of CL. The total molecular weight per molecule (M_n^{NMR}) is calculated by $M_{arm}^{NMR}=3760+M_{arm}^{NMR}\times 29.2$. For LPCL samples, M_{arm}^{NMR} is calculated from the integration area of the peak corresponding to methylene groups in CL units (–$COCH_2$–, δ 2.40–2.70, $b+b'$ in Fig. 1(c)) to that of the peak corresponding to the methylene groups from ethylene glycol (–COO–CH_2–CH_2–OCO–, δ 4.50–4.60, a in Fig. 1(c)) according to $M_{arm}^{NMR}=2I_{b+b'}/I_a\times 114.14$. M_{arm}^{NMR} is taken as M_n^{NMR} since that linear PCL is considered as a single chain. The calculated results are summarized in Table 1.

The molecular weights of SHPCL and LPCL both increase almost linearly with the [CL]/[OH] ratio as shown in Table 1. The increase of molecular weight with [CL]/[OH] is especially distinct since average about 29.2 arms are growing from one SBOH as mentioned above. For SHPCL samples, since the outer PCL layer is further away from the silsesquioxane core with arm length increasing and thus the crowding of the most outer PCL layer deceases, the –OH end-groups located at the surface of SHPCL intermediate with longer PCL arms will have more free space and higher probability to initiate the polymerisation of CL monomer. As a result, the difference of molecular weight for the final products resulted from the SHPCL intermediates with longer and shorter PCL arms will become larger, namely, the molecular weight distribution becomes broader with the [CL]/[OH] ratio increased. It also can be found from Fig. 2 that two peaks in the GPC spectra appeared as the [CL]/[OH] ratio increased to 10. The similar phenomenon in GPC spectra is often observed in the preparation of branched polymers growing from a central core [36,37]. The bimodal distribution may be due to the irregularity of initial PCL arm number initiated from SBOH since the hydroxyl groups on SBOH is very dense and crowding (58.4 hydroxyl groups per SBOH). The polymerisation propagation of CL monomer from SHPCL intermediate molecules with more arms is slower than that from SHPCL intermediate molecules with less arms due to steric hindrance. When the [CL]/[OH] ratio is low, the overall molecular weight for SHPCL with less arms is lower than that

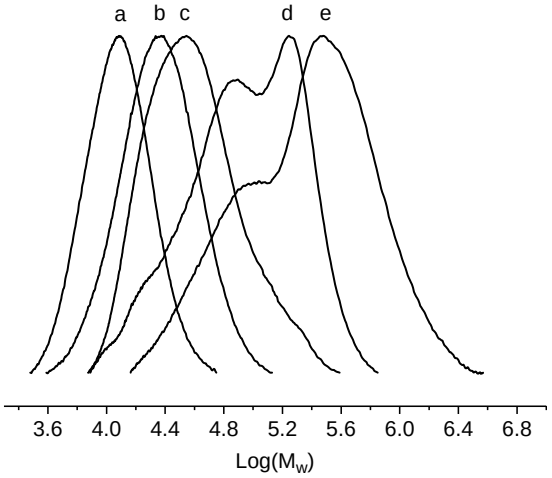

Fig. 2. GPC curves of SHPCLs and LPCLs : (a) LPCL-25, (b) LPCL-35, (c) SHPCL-4, (d) SHPCL-10, (e) SHPCL-40.

for SHPCL with more arms; When the [CL]/[OH] ratio is high enough, the overall molecular weight for SHPCL with less arms gradually becomes higher than that for SHPCL with more arms instead. Moreover, as the [CL]/[OH] ratio further increased from 10 to 40 (the curves d to e in Fig. 2), the increases of the left peak indicating lower molecular weight is more slow than that of the right peak indicating higher molecular weight, which should correspond to that the growth of SHPCL molecules with more arms is more restricted than that with less arms. The transesterification and increasing viscosity are also possible causes for the broadening of molecular weight distribution. Further study about the detailed mechanism of broadening of molecular weight distribution is still ongoing, which is beyond the scope of this work.

The number average molecular weights calculated from ^{1}H NMR spectra (M_n^{NMR}) are much lower than the measured M_n values from GPC (M_n^{GPC}) for LPCLs, while M_n^{NMR} of SHPCLs are much higher than M_n^{GPC}. Due to the compact spheric structure of star and branched polymers, GPC measurements usually underestimate their real molecular weights since GPC instruments are calibrated with linear polymers [38]. It is reasonable to conclude that SHPCLs have compact spherical architectures from the contrast of GPC results between SHPCLs and LPCLs and the initial hard spherical structure of SBOH (Scheme 1).

SHPCLs and LPCLs were prepared to have appropriate molecular weights for the comparison of crystallization kinetics. All SHPCLs have higher molecular weights than LPCLs, i.e. for M_n^{NMR} or M_n^{GPC}, LPCL-25 < LPCL-35 < SHPCL-4 < SHPCL-10 < SHPCL-40; and the sequence of average molecular weight per arm (M_{arm}^{NMR}) of SHPCLs and LPCLs is as follows: SHPCL-4 < SHPCL-10 < LPCL-25 < LPCL-35 < SHPCL-40, as listed in Table 1.

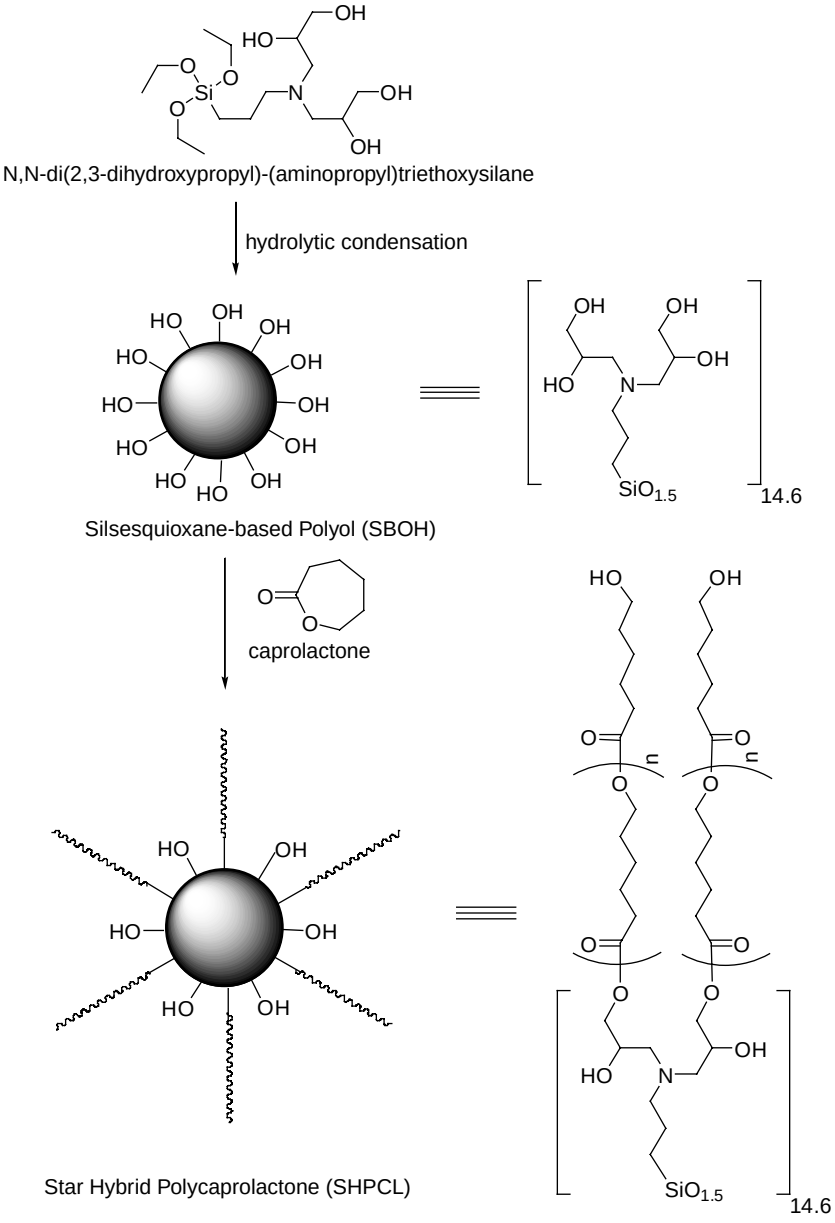

Scheme 1. Synthesis route of SHPCLs.

3.2. Non-isothermal crystallization kinetics

The non-isothermal DSC measurements were performed to characterize the crystallization behaviours of SHPCLs with different arm length and LPCLs for comparison. The samples were subjected to the thermal treatments as described in the measurement section and the crystallization exothermic curves were recorded. The measured heat flow curves against temperatures at different cooling rates (from 10 to 2 °C/min) are shown in Fig. 3. All samples showed similar crystallization exothermic curves and similar change of curves with the cooling rates, indicating that they have similar crystallization mechanism.

Fig. 4 shows the illustration of crystallization parameters used to describe the crystallization behaviours of SHPCLs and LPCLs [39], including (1) T_s, the starting crystallization temperature, taking from the point where the heat flow curve begins to decrease below zero; (2) T_e, the ending temperature of crystallization, taking from the point where the heat flow becomes zero again; (3) T_p, the peak temperature, taking from the point where the heat flow reaches the max; (4) ΔT, the width of temperature at the half height of the heat flow curve. The analyzed results from Fig. 3 are summarized in Table 2. T_s, T_e and T_p shift to lower temperature for all samples with increasing the cooling rate, indicating faster cooling rate results

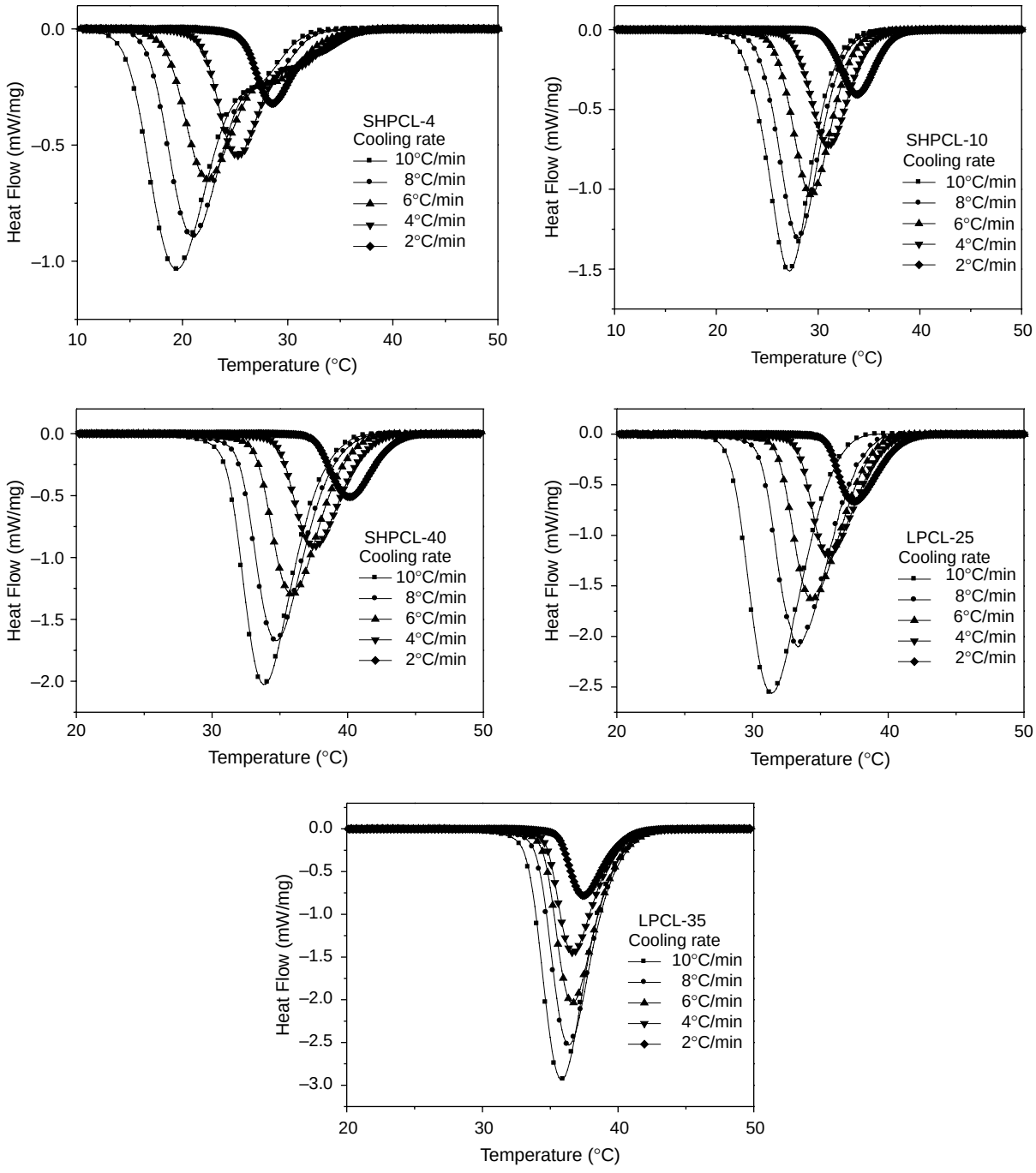

Fig. 3. Non-isothermal crystallization exothermal curves of SHPCLs and LPCLs.

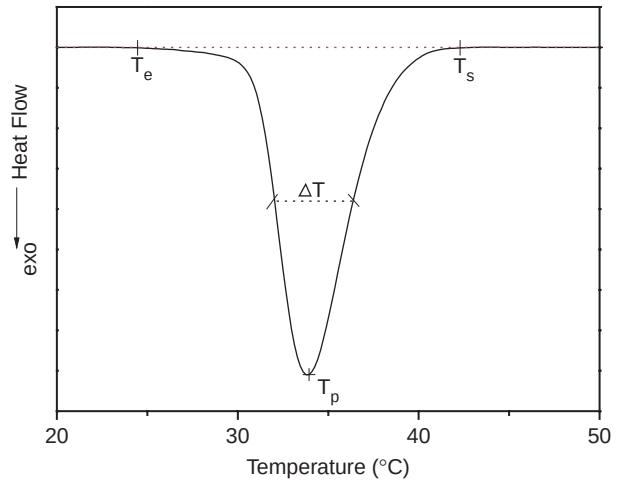

Fig. 4. Schematic illustration of crystallization parameters listed in Table 2.

in more evident super-cooling. At a given cooling rate, T_s, T_e and T_p increase as the molecular weight increases for SHPCL series or LPCL series, respectively. However, the T_s, T_e and T_p of SHPCL-4 and SHPCL-10 are much lower than that of LPCL-25 and LPCL-35, although the former two have much higher total molecular weights (M_n^{NMR}) than the later two. At a given cooling rate, T_s, T_e and T_p of all samples are in the order as: SHPCL-4 < SHPCL-10 < LPCL-25 < SHPCL-40 ≈ LPCL-35, which is almost consistent with molecular weight of per arm (M_{arm}^{NMR}) in Table 1.

ΔT is a parameter to evaluate the distribution of crystal dimensions, and the smaller the ΔT, the narrower the distribution. ΔT is greatly affected by cooling rate. For a given sample, the ΔT broadens as the cooling rate increases, suggesting that the nucleation process is dominative in the steps of nucleation and growth model of PCL crystal. The arm length also has a pronounced effect on ΔT, SHPCL with shorter PCL arms has much broader ΔT at a given cooling rate as shown in Table 2. This indicates that the formed crystals of SHPCL with shorter PCL arm are less perfect than that from SHPCL with longer PCL arm.

To evaluate quantitatively the influence of inorganic silsesquioxane-based core and star architecture on the extent of crystallization of PCL, the crystalline heat of samples (ΔH_c) was calculated according to the formula (1) from the measurement of heat flow rate vs time.

$$\Delta H_c = \int_{t1}^{t2} (dH_c/dt)dt \quad (1)$$

Where t_1 and t_2 are the starting and the ending time of crystallization, corresponding to the temperatures of T_s and T_e, respectively. The crystallinity, X_c, was calculated using the formula (2) as follow:

Table 2
Crystallization parameters of SHPCLs and LPCLs

Sample	Crystallization parameter	Cooling rate (°C/min)				
		10	8	6	4	2
SHPCL-4	T_s (°C)	35.2	36.6	38.3	38.6	39.7
	T_e (°C)	10.8	13.2	15.1	17.9	21.3
	T_p (°C)	19.5	21.0	22.4	25.3	28.6
	ΔT (°C)	6.57	6.03	5.83	4.81	4.17
	ΔH_c (J/g)	−51.0	−51.0	−52.1	−53.2	−53.2
	X_c (%)	37.4	37.4	38.2	39.0	39.0
SHPCL-10	T_s (°C)	37.5	37.9	38.6	41.4	41.6
	T_e (°C)	15.0	17.0	18.4	21.3	27.4
	T_p (°C)	27.2	28.0	29.3	31.1	33.8
	ΔT (°C)	4.81	4.49	4.34	4.17	3.85
	ΔH_c (J/g)	−51.7	−52.2	−52.1	−52.6	−52.8
	X_c (%)	37.9	38.3	38.2	38.6	38.7
SHPCL-40	T_s (°C)	42.3	42.4	43.4	46.2	47.1
	T_e (°C)	24.5	23.4	26.5	27.9	34.5
	T_p (°C)	33.9	34.7	35.9	37.5	40.1
	ΔT (°C)	4.01	3.98	3.95	3.79	3.44
	ΔH_c (J/g)	−58.0	−58.7	−58.8	−58.8	−59.0
	X_c (%)	42.5	43.0	43.1	43.1	43.2
LPCL-25	T_s (°C)	38.9	42.3	42.4	42.7	43.6
	T_e (°C)	24.9	25.1	24.8	26.6	32.1
	T_p (°C)	31.4	33.5	34.4	35.6	37.5
	ΔW (°C)	4.55	4.24	4.04	3.66	3.25
	ΔH_c (J/g)	−74.1	−74.2	−73.1	−73.3	−72.0
	X_c (%)	54.3	54.4	53.6	53.8	52.8
LPCL-35	T_s (°C)	43.7	44.9	47.5	44.6	46.0
	T_e (°C)	27.1	27.2	27.6	28.1	29.9
	T_p (°C)	35.8	36.4	36.6	36.7	37.5
	ΔW (°C)	3.53	3.32	3.24	3.04	2.78
	ΔH_c (J/g)	−73.9	−76.6	−78.5	−78.6	−78.9
	X_c (%)	54.2	56.2	57.5	57.6	57.8

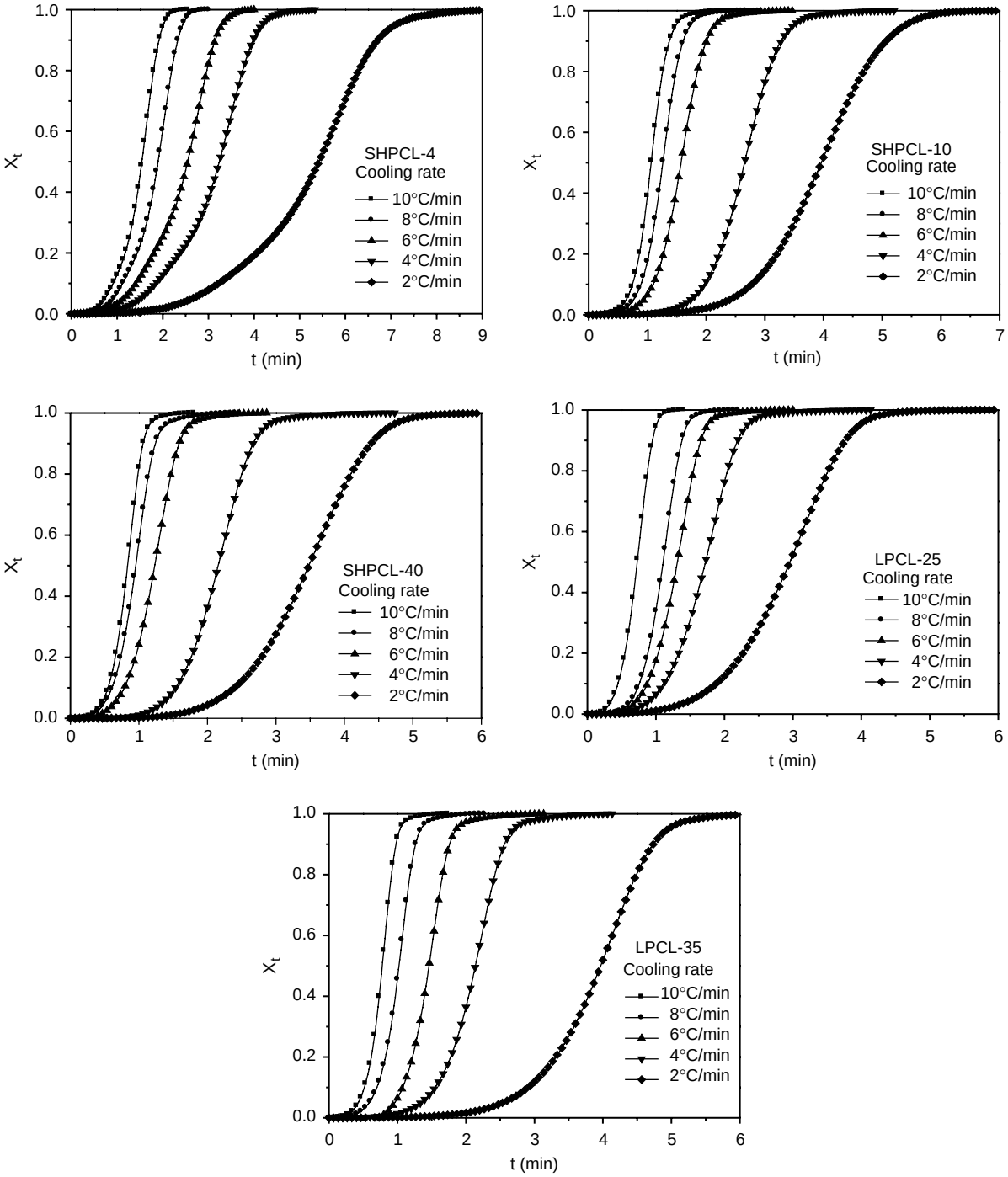

Fig. 5. Plots of relative crystallinity, X_t vs crystallization time, t, for SHPCLs and LPCLs.

$$X_c(\%) = \frac{\Delta H_c}{\Delta H_c^0} \times 100 \quad (2)$$

Where ΔH_c^0 is the heat of crystallization for a 100% crystalline poly(ε-caprolactone), which is 136.4 J/g. As summarized in Table 2, the ΔH_c and the corresponding X_c for SPHCLs increase with increasing the arm length at a given cooling rate. The ΔH_c and the corresponding X_c for LPCLs also increase with increasing the molecular weight. However, the ΔH_c and the corresponding X_c for SPHCLs are much lower than that of LPCLs although SHPCLs have higher molecular weights than LPCLs. Moreover, although the M_{arm}^{NMR} of SHPCL-40 is even higher than the M_n^{NMR} of LPCL-25 and LPCL-40, the former has lower ΔH_c and corresponding X_c than the later two. These results indicate that the crystallinity of PCL arms is greatly reduced by the silsesquioxane-based inorganic core and the star architecture.

Besides, the above study about the influence of inorganic core and the star architecture on the extent of

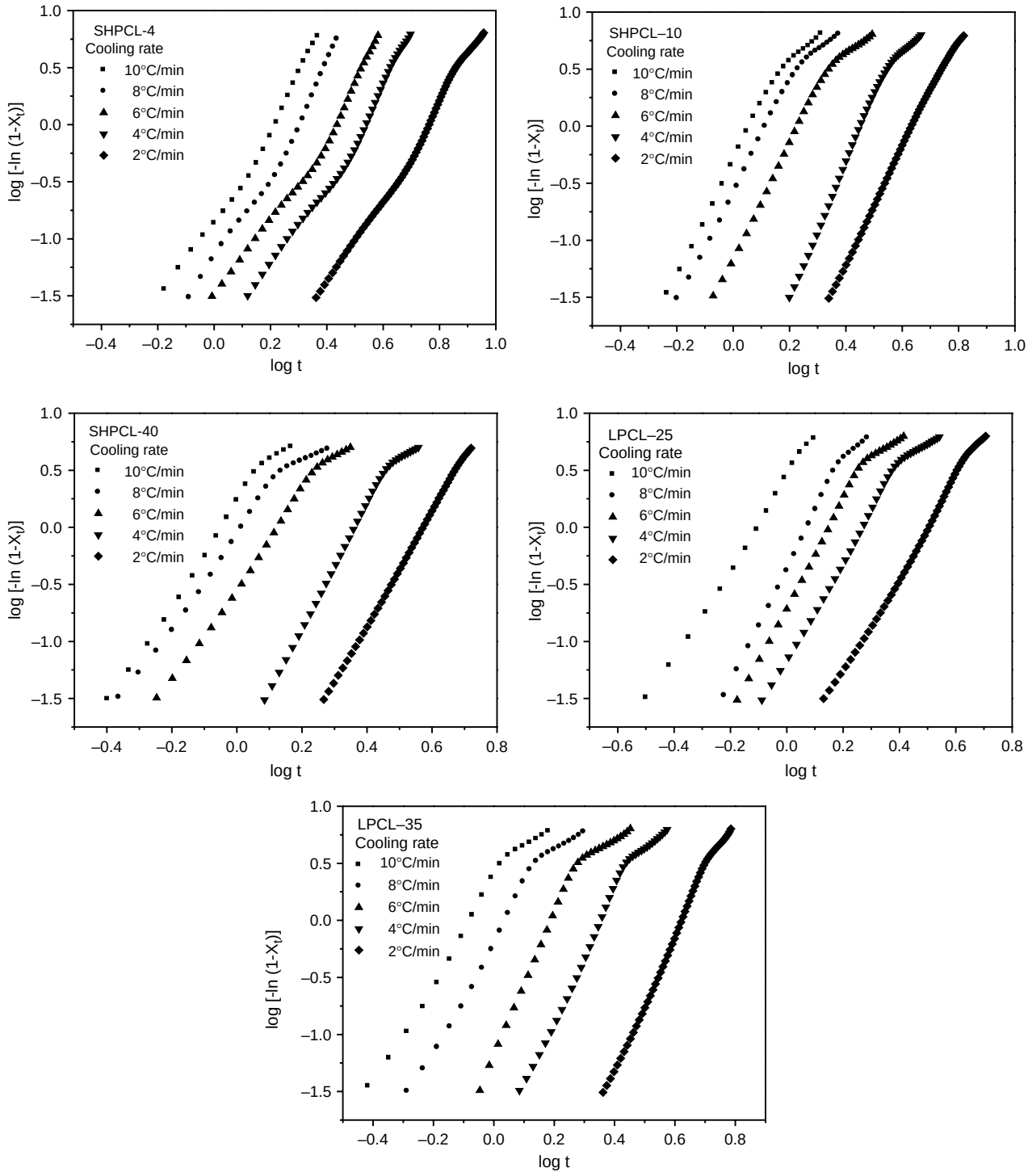

Fig. 6. Plots of $\log[-\ln(1-X_t)]$ vs $\log t$ for SHPCLs and LPCLs.

crystallization, their influence on the process of crystallization was studied by further crystallization kinetics analysis.

Integration of the exothermal peak during the non-isothermal scan give the relative crystallinity (X_t) as a function of temperature, which can be transformed into a function of time according to formula (3) as follows:

$$X_t = \frac{\int_{t1}^{t} (\mathrm{d}H_c/\mathrm{d}t)\mathrm{d}t}{\Delta H_c} \tag{3}$$

Fig. 5 shows the X_t curves against time t for all samples. For a given sample, the time for X_t to reach 100% is longer at a slower cooling rate, implying the nucleation is the dominating

Table 3
Parameters of crystallization kinetics of SHPCLs and LPCLs

Sample	Avrami analysis	Cooling rate (°C/min)				
		10	8	6	4	2
SHPCL-4	K	0.14	0.056	0.024	0.0077	8.0×10^{-4}
	n	4.19	4.29	3.89	4.06	4.11
	K_c	0.82	0.70	0.54	0.30	0.028
	$t_{1/2}$	0.96	1.00	1.07	1.23	2.18
SHPCL-10	K	0.45	0.26	0.087	0.0039	6.8×10^{-4}
	n	4.30	4.24	4.22	5.13	4.95
	K_c	0.92	0.85	0.67	0.25	0.026
	$t_{1/2}$	0.94	0.95	1.01	1.22	1.94
SHPCL-40	K	1.64	0.87	0.300	0.0104	0.0015
	n	4.51	4.14	4.25	5.43	4.92
	K_c	1.05	0.98	0.82	0.32	0.038
	$t_{1/2}$	0.91	0.92	0.96	1.15	1.80
LPCL-25	K	2.66	0.41	0.209	0.0799	0.00727
	n	3.99	4.62	4.07	3.86	4.27
	K_c	1.10	0.90	0.77	0.53	0.085
	$t_{1/2}$	0.89	0.95	0.97	1.07	1.63
LPCL-35	K	1.74	0.565	0.103	0.0142	2.30×10^{-4}
	n	3.97	4.12	4.53	4.98	5.80
	K_c	1.06	0.93	0.68	0.34	0.015
	$t_{1/2}$	0.90	0.93	1.00	1.15	1.93

step in the crystallization process. The time for X_t to reach 100% for SHPCLs are longer than LPCLs at a given cooling rate, indicating that the inorganic core and star architecture slow down the crystallization rate.

Several theoretical methods have been proposed to predict and analyze non-isothermal crystallization kinetics [39,40]. In this work, we employed the Avrami equation for the analysis of crystallization kinetics for SHPCL and LPCL series. On the basis of the assumption that the non-isothermal crystallization is the result of infinite isothermal processes, the primary non-isothermal stage could be described by the Avrami equation (formula (4)) as follows:

$$1-X_t = \exp(-Kt^n) \tag{4}$$

K is the overall crystallization rate constant and is temperature dependent; n is the Avrami index, including the information on nucleation and growth geometry.

To compare the crystallization rate in a straight-forward way, the K and n values are derived from the double-logarithmic form of formula (4) according to formula (5) as follows:

$$\log[-\ln(1-X_t)] = \log K + n\log t \tag{5}$$

Fig. 6 shows the $\log[-\ln(1-X_t)]$ vs $\log t$ curves for all samples. A good linear relationship can be found between $\log[-\ln(1-X_t)]$ and $\log t$ in a wide range of crystallinity, implying that Avrami equation is suitable for the kinetics study. The $\log K$ and n are taken from the intercept and the slope of linear fitting of the $\log[-\ln(1-X_t)]$ vs $\log t$ curves, respectively. The resulted K and n values are summarized in Table 3. Taking into account the effect of cooling rate on crystallization kinetics, the K value must be properly corrected to obtain the corrected crystallization rate constant K_c according to formula (6) as follows:

$$\log K_c = \frac{\log K}{\chi} \tag{6}$$

where χ is the cooling rate. As listed in Table 3, SHPCLs have lower K_c values than LPCLs, which have been discussed above. Moreover, it was found that the K_c value of LPCLs decreases slightly as the molecular weight increases, which is also observed by other groups [22]. However, the K_c value of SHPCLs increases with increasing the molecular weight. Since the molecular weight has two opposing effects on the crystallization rate: one is to reduce the segmental mobility, which would result in retardation of crystallization rate, while the other is to increase the degree of super-cooling, which would promote nucleation and thus increase crystallization rate. Thus, it can be concluded that the unique architecture of SHPCL compensates the negative effect of increasing molecular weight on crystallization rate, which should be ascribed to that the interaction of many long PCL arms connected to a central core is helpful for crystallization. For SHPCLs in the studied molecular weight range, the sample with longer arm crystallizes in faster rate, which can be observed in the morphology study as below.

The $t_{1/2}$ in Table 3 is the crystallization half-time, defined as the time at which the extent of crystallization is complete by 50%. It is determined by K_c and n by formula (7) as follows [39]:

$$t_{1/2} = \left(\frac{\ln 2}{K_c}\right)^{1/n} \tag{7}$$

Taking into account that the reciprocal of $t_{1/2}$ is also the reflection of overall crystallization rate, $t_{1/2}$ values show reverse trend as K_c as listed in Table 3. The discussion about K_c is also suitable for $t_{1/2}$.

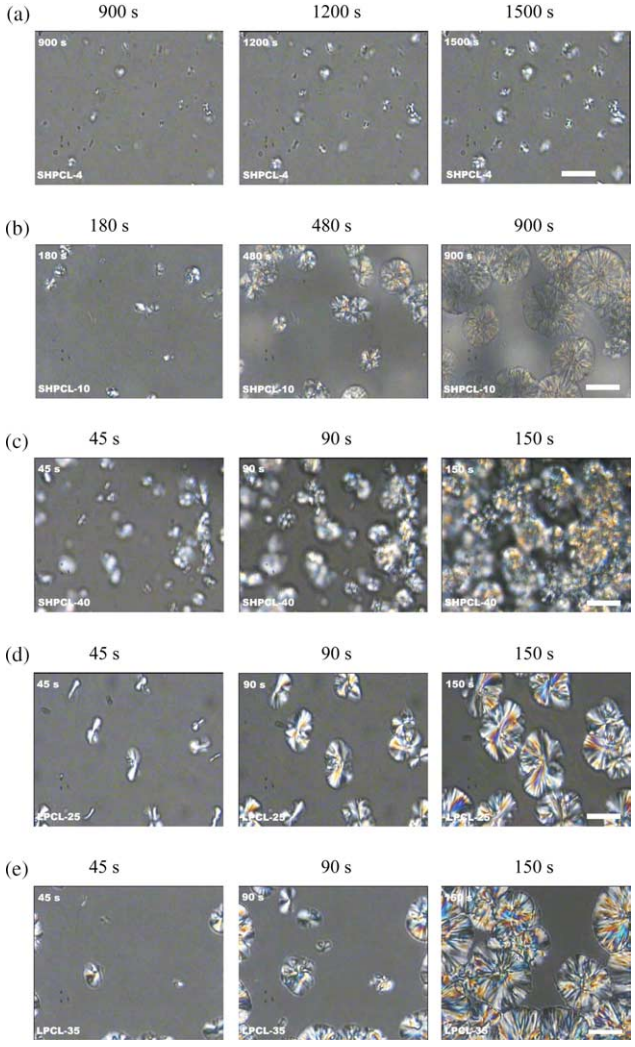

Fig. 7. Polarized optical micrographs at different time crystallizing at 40 °C for (a) SHPCL-4, (b) SHPCL-10, (c) SHPCL-40, (d) LPCL-25, (e) LPCL-35 (all white bars in images are 40 μm).

The n values for HPCLs and LPCLs are ranging from 3.8 to 5.8 and seem not to depend on the molecular architecture and composition. Since n is a complicate and not straightforward parameter, which is affected by a lot of factors such as volume changes due to phase transformation, incomplete crystallization, annealing, or different mechanisms involved during the process [41]. It is difficult to draw any reliable relationship between n and the molecular architecture and composition at present.

3.3. Morphological observation

DSC and POM are two complementary techniques to investigate the crystallization process. What the calorimetric data from non-isothermal DSC measurements reflects are the overall crystallinity and the overall crystallization rate, whereas POM can provide intuitionistic information about the development of spherulites in terms of both nucleation and growth. The real time crystallization process of SHPCLs and LPCLs was observed by POM equipped with a video camera by cooling their melt at the integrated hot stage at 40 °C. The images of spherulites at different crystallization time are shown in Fig. 7. It can be found that the nucleation of SHPCL-4 and SHPCL-10 is difficult. Although the total molecular weights of SHPCL-4 and SHPCL-10 are much larger than that of LPCL-25 and LPCL-35, it took much longer time for the formers to nucleate than the laters, indicating the inorganic silsesquioxane-based core greatly inhibit nucleation when the PCL arms are not longer enough. Because these PCL arms are in very close vicinity due to their covalent attachment to the core, when the PCL arms are long enough, they can interact with each other to form initial ordering for nucleation, so SHPCL-40 forms very dense and small spherulites quickly as shown in Fig. 7.

The crystallization is usually a two-step process: nucleation and crystal growth. The nucleation rate can be reflected by the time when visible spherulites can be observed, which is in the order as: SHPCL-4»SHPCL-10»LPCL-25 > LPCL-

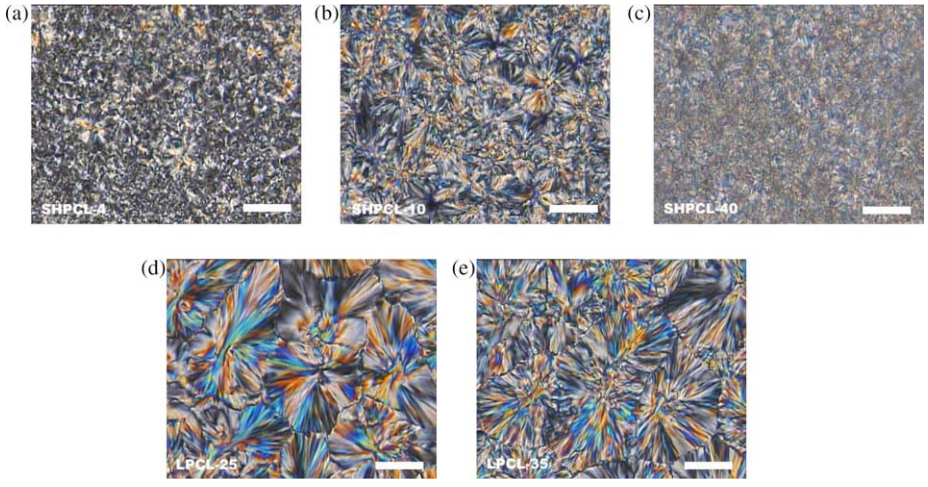

Fig. 8. Polarized optical micrographs after crystallizing at 40 °C for 10 h for (a) SHPCL-4, (b) SHPCL-10, (c) SHPCL-40, (d) LPCL-25, (e) LPCL-35 (All white bars in images are 40 μm).

35 ≈ SHPCL-40. It is almost consistent with the overall crystallization rate from the non-isothermal DSC measurements, implying again that the nucleation is the key step in the crystallization process.

The morphology of crystal is thought to be dependent on not only the mechanism and rate of nucleation, but also the subsequent growth rate of the spherulites [42]. Because of that the morphologies of SHPCL spherulites are varied with arm length as shown in Fig. 7, the growth rate of SHPCL spherulite radius are difficult to evaluate quantitatively. However, it is obvious that the growth is difficult for SHPCL-4 due to the disturbance of inorganic core and branched star architecture. The disturbance was weakened as the arm length increased, so SHPCL-10 forms the spherulites with better dimensional regularity than SHPCL-4, which is consistent with the ΔT result in DSC measurement.

Fig. 8 shows the final polarized optical micrographs of SHPCLs and LPCLs after crystallizing at 40 °C for 10 h. All samples are completely volume filled with crystals after standing for such a long enough time. The inorganic core and star architecture of SHPCL samples have great influence on their crystal morphologies. The morphologies of SHPCL-4 are coarsest and almost no regular crystal can be observed. With the arm length increases, SHPCL-10 forms a relative larger and more perfect crystal with Maltese cross. As the arm length continues to increase, SHPCL-40 forms a very dense and small crystal. In the SHPCL samples, SHPCL-10 showed the most perfect crystal morphology, but its crystal morphologies is still not as perfect as that of LPCL samples. The spherulites in LPCLs are regular in shape with neat borders and display fibrous crystals radiating from central points and a well-defined Maltese cross, whereas the spherulites in SHPCL-10 are smaller and more dendritic than that of LPCLs.

4. Conclusions

A series of SHPCLs were prepared from ROP of CL initiated by SBOH and LPCLs as linear polymers were also prepared for comparison. From the ^{1}H NMR measurements, the initiating degree of hydroxyl groups on SBOH for ROP was calculated to be about 50%. The ^{1}H NMR and GPC measurements both showed that the total molecular weight increased almost linearly with the ratio of [CL]/[OH] as given in the order of LPCL-25 < LPCL-35 < SHPCL-4 < SHPCL-10 < SHPCL-40.

At a given cooling rate, the T_s, T_e and T_p were determined to be in the order as: SHPCL-4 < SHPCL-10 < LPCL-25 < SHPCL-40 ≈ LPCL-35, which is not consistent with total molecular weight but with the arm length, further supporting the branched star architecture of SHPCL. The ΔT values of SHPCL-4 and SPHCL-10 are broader than LPCL-25 and LPCL-35, even though that the molecular weights of the formers are higher than the laters. The crystallinity X_c calculated from heat flow followed the order as: SHPCL-4 < SHPCL-10 < SHPCL-40 < LPCL-25 < LPCL-35. These results indicate that the inorganic core and star architecture greatly influence the ordering of segments during the crystallization.

The kinetics analysis by Avrami equation showed a good linear relationship between $\log[-\ln(1-X_t)]$ vs $\log t$. The corrected overall crystallization rate constant (K_c) were found to be in the order as: SHPCL-4 < SHPCL-10 < LPCL-35 < LPCL-25 ≈ SHPCL-40, indicating that the inorganic core and star architecture greatly reduced crystallization rate when the arms are short, whereas the unique architecture helps crystallization for SHPCL with longer arms. The results from polarized light microscopy indicate that the nucleation is the key step during the crystallization process for SHPCL samples. It's difficult for SHPCL samples with short PCL arms to nucleate, however, since these PCL arms are in very close vicinity due to their covalent attachment to the core, when the arms are long enough to interact with each other, the unique star architecture is in favour of nucleation.

The crystallization kinetics study of SHPCL samples has given a guidance for designing novel hybrid PCL with high functionality and molecular weight but low crystallinity as potential materials in tissue engineering fields.

Acknowledgements

This work has been supported by China NKBRSF Project (2001CB409600) and National Natural Science Foundation of China (50233030).

References

[1] Heuschen J, Jerome R, Teyssie P. Macromolecules 1981;14:242–6.
[2] Allen C, Han JN, Yu YS, Maysinger D, Eisenberg A. J Controlled Release 2000;63:275–86.
[3] Amsden B, Wang S, Wyss U. Biomacromolecules 2004;5:1399–404.
[4] Amsden BG, Misra G, Gu F, Younes HM. Biomacromolecules 2004;5:2479–86.
[5] Barbato F, La Rotonda MI, Maglio G, Palumbo R, Quaglia F. Biomaterials 2001;22:1371–8.
[6] Guan HL, Xie ZG, Tang ZH, Xu XY, Chen XS, Jing XB. Polymer 2005;46:2817–24.
[7] Cohn D, Salomon AF. Biomaterials 2005;26:2297–305.
[8] Huang MH, Li SM, Vert M. Polymer 2004;45:8675–81.
[9] Zhu G, Li Y, Yin J, Ling J, Shen Z. J Therm Anal Calorim 2004;77:833–7.
[10] Nagata M, Sato Y. J Polym Sci, Part A: Polym Chem 2005;43:2426–39.
[11] Teng CQ, Kai Y, Ping J, Yu MH. J Polym Sci, Part A: -Polym Chem 2004;42:5045–53.
[12] Nunez E, Gedde UW. Polymer 2005;46:5992–6000.
[13] Nunez E, Ferrando C, Malmstrom E, Claesson H, Werner PE, Gedde UW. Polymer 2004;45:5251–63.
[14] Claesson H, Malmstrom E, Johansson M, Hult A. Polymer 2002;43:3511–8.
[15] Inoue K. Prog Polym Sci 2000;25:453–571.
[16] McKee MG, Unal S, Wilkes GL, Long TE. Prog Polym Sci 2005;30:507–39.
[17] Malmstrom E, Hult A. J Macromol Sci Rev Macromol Chem Phys 1997;C37:555–79.
[18] Lang MD, Wong RP, Chu CC. J Polym Sci, Part A: Polym Chem 2002;40:1127–41.
[19] Filali M, Meier MAR, Schubert US, Gohy JF. Langmuir 2005;21:7995–8000.
[20] Qiu ZB, Yang WT, Ikehara T, Nishi T. Polymer 2005;46:11814–9.
[21] Kuo SW, Chan SC, Chang FC. J Polym Sci Part B: Polym Phys 2004;42:117–28.

[22] Zheng SX, Zheng HF, Guo QP. J Polym Sci, Part B-Polym Phys 2003;41: 1085–98.
[23] Guo QP, Groeninckx G. Polymer 2001;42:8647–55.
[24] Nunez E, Ferrando C, Malmstrom E, Claesson H, Gedde UW. J Macromol Sci-Phys 2004;B43:1143–60.
[25] Choi J, Kwak SY. Macromolecules 2004;37:3745–54.
[26] Homminga D, Goderis B, Dolbnya I, Groeninckx G. Polymer 2006;47: 1620–9.
[27] Mackenzie JD, Bescher EP. J Sol–Gel Sci Technol 1998;13:371–7.
[28] Wen JY, Wilkes GL. Chem Mater 1996;8:1667–81.
[29] Nie KM, Pang WM, Zheng SX, Wang YS, Lu F, Zhu QR. Polym Int 2005; 54:327–35.
[30] Rhee SH. Biomaterials 2004;25:1167–75.
[31] Jiang SC, Ji XL, An LJ, Jiang BZ. Polymer 2001;42:3901–7.
[32] Di E. Polymer 2004;45:8893–900.
[33] Chan SC, Kuo SW, Chang FC. Macromolecules 2005;38:3099–107.
[34] Mori H, Lanzendorfer MG, Muller AHE, Klee JE. Macromolecules 2004; 37:5228–38.
[35] Mori H, Muller AHE, Klee JE. J Am Chem Soc 2003;125:3712–3.
[36] Lin D, Shi WF, Nie KM, Zhang YC. J Appl Polym Sci 2001;82: 1630–6.
[37] Shi WF, Ranby B. J Appl Polym Sci 1996;59:1937–44.
[38] Yu D, Vladimirov N, Frechet JMJ. Macromolecules 1999;32:5186–92.
[39] Di Lorenzo ML, Silvestre C. Prog Polym Sci 1999;24:917–50.
[40] Qiu ZB, Ikehara T, Nishi T. Polymer 2003;44:5429–37.
[41] Chuah KP, Gan SN, Chee KK. Polymer 1999;40:253–9.
[42] Chen HL, Li LJ, OuYang WC, Hwang JC, Wong WY. Macromolecules 1997;30:1718–22.